HHS Public Access

Author manuscript

J Neurosurg. Author manuscript; available in PMC 2022 July 01.

Published in final edited form as:

J Neurosurg. 2022 January 01; 136(1): 88–96. doi:10.3171/2021.1.JNS203536.

Use of predictive spatial modeling to reveal that primary cancers have distinct central nervous system topography patterns of brain metastasis

Josh Neman, PhD[1,2,3,6,8], **Meredith Franklin, PhD**[4,6], **Zachary Madaj, MS**[7], **Krutika Deshpande, MS**[1,6], **Timothy J. Triche Jr., PhD**[7], **Gal Sadlik, MS**[1,6], **John D. Carmichael, MD**[1,6,8], **Eric Chang, MD**[3,5,6,8], **Cheng Yu, PhD**[1,6,8], **Ben A. Strickland, MD**[1,6], **Gabriel Zada, MD**[1,3,6,8]

[1]Department of Neurological Surgery, University of Southern California, Los Angeles, California

[2]Department of Physiology and Neuroscience, University of Southern California, Los Angeles, California

[3]Norris Comprehensive Cancer Center, University of Southern California, Los Angeles, California

[4]Department of Preventive Medicine, University of Southern California, Los Angeles, California

[5]Department of Radiation Oncology, University of Southern California, Los Angeles, California

[6]Keck School of Medicine, University of Southern California, Los Angeles, California

[7]Department of Bioinformatics, Van Andel Institute, Grand Rapids, Michigan

[8]USC Brain Tumor Center, University of Southern California, Los Angeles, California

Abstract

OBJECTIVE—Brain metastasis is the most common intracranial neoplasm. Although anatomical spatial distributions of brain metastasis may vary according to primary cancer subtype, these patterns are not understood and may have major implications for treatment.

METHODS—To test the hypothesis that the spatial distribution of brain metastasis varies according to cancer origin in nonrandom patterns, the authors leveraged spatial 3D coordinate data derived from stereotactic Gamma Knife radiosurgery procedures performed to treat 2106 brain metastases arising from 5 common cancer types (melanoma, lung, breast, renal, and colorectal).

Correspondence: Josh Neman: University of Southern California, Los Angeles, CA. yebrahim@usc.edu.

Author Contributions

Conception and design: Neman, Chang, Zada. Acquisition of data: all authors. Analysis and interpretation of data: Neman, Franklin, Madaj, Deshpande, Triche, Sadlik, Carmichael, Chang, Yu, Zada. Drafting the article: Neman, Franklin, Madaj, Deshpande, Triche, Sadlik, Carmichael, Chang, Yu, Zada. Critically revising the article: Neman, Triche, Carmichael, Chang, Yu, Zada. Reviewed submitted version of manuscript: Neman, Chang, Strickland, Zada. Approved the final version of the manuscript on behalf of all authors: Neman. Administrative/technical/material support: Neman, Zada. Study supervision: Neman, Zada.

Disclosures

The authors report no conflict of interest concerning the materials or methods used in this study or the findings specified in this paper.

Supplemental Information

Online-Only Content

Supplemental material is available with the online version of the article.

Supplemental Material. https://thejns.org/doi/suppl/10.3171/2021.1.JNS203536.

Two predictive topographic models (regional brain metastasis echelon model [RBMEM] and brain region susceptibility model [BRSM]) were developed and independently validated.

RESULTS—RBMEM assessed the hierarchical distribution of brain metastasis to specific brain regions relative to other primary cancers and showed that distinct regions were relatively susceptible to metastasis, as follows: bilateral temporal/parietal and left frontal lobes were susceptible to lung cancer; right frontal and occipital lobes to melanoma; cerebellum to breast cancer; and brainstem to renal cell carcinoma. BRSM provided probability estimates for each cancer subtype, independent of other subtypes, to metastasize to brain regions, as follows: lung cancer had a propensity to metastasize to bilateral temporal lobes; breast cancer to right cerebellar hemisphere; melanoma to left temporal lobe; renal cell carcinoma to brainstem; and colon cancer to right cerebellar hemisphere. Patient topographic data further revealed that brain metastasis demonstrated distinct spatial patterns when stratified by patient age and tumor volume.

CONCLUSIONS—These data support the hypothesis that there is a nonuniform spatial distribution of brain metastasis to preferential brain regions that varies according to cancer subtype in patients treated with Gamma Knife radiosurgery. These topographic patterns may be indicative of the abilities of various cancers to adapt to regional neural microenvironments, facilitate colonization, and establish metastasis. Although the brain microenvironment likely modulates selective seeding of metastasis, it remains unknown how the anatomical spatial distribution of brain metastasis varies according to primary cancer subtype and contributes to diagnosis. For the first time, the authors have presented two predictive models to show that brain metastasis, depending on its origin, in fact demonstrates distinct geographic spread within the central nervous system. These findings could be used as a predictive diagnostic tool and could also potentially result in future translational and therapeutic work to disrupt growth of brain metastasis on the basis of anatomical region.

Keywords

brain metastasis; topography; Gamma Knife; spatial distribution; oncology; stereotactic radiosurgery

Brain metastasis arises in the CNS after the spread of circulating mesenchymal cells from primary tumors. The lifetime incidence of brain metastasis in cancer patients is 20%–45%.[1] Lung, breast, melanoma, colorectal, and renal cancers show the highest metastatic proclivity for the brain, followed less commonly by thyroid, gastrointestinal, and prostate cancers. Although accumulating evidence underscores the importance of the brain microenvironment in the establishment and progression of metastasis, there nevertheless remains ambiguity as to whether CNS metastasis arises and progresses according to preferential anatomical spatial distributions based on the primary cancer of origin.[2,3] Gamma Knife radiosurgery (GKRS) is a minimally invasive, targeted form of stereotactic radiosurgery used to treat brain tumors and other lesions. GKRS and other forms of stereotactic radiosurgery are the first line of treatment for many patients with newly diagnosed brain metastasis, especially those with small metastasis not considered an ideal surgical target. GKRS offers the benefits of highly accurate, single-fraction, frame-based radiosurgery with reduced incidence of cognitive dysfunction when compared with whole-brain radiation.[4]

In this study, we harnessed stereotactic coordinate information from a unique data set of over 2000 brain metastases arising from 5 common primary cancer types (breast, colorectal, lung, melanoma, and renal) in patients treated with GKRS. Based on highly specific patient and metastatic tumor coordinates, two prediction models were developed to test the hypothesis that brain metastasis is not randomly distributed within the CNS and varies according to primary cancer origin. A regional brain metastasis echelon model (RBMEM) was developed to test whether, given a preselected brain region, one particular cancer subtype showed relative predilection for metastasis. A brain region susceptibility model (BRSM) was then utilized to assess whether a given primary cancer subtype was more likely to metastasize to certain brain regions, independent of other cancer types. Our findings suggest that nonuniform, preferential topographic patterns of brain metastasis exist and vary probabilistically according to primary cancer origin in patients treated with GKRS.

Methods

Description of Patients

After approval from the USC IRB, data were retrospectively collected about patients with metastatic brain cancer treated using single-fraction GKRS at USC Keck Medical Center from 1994 to 2015. As a part of the GKRS procedure, all patients were placed in a stereotactic Leksell coordinate head frame using standardized head fixation after application of local anesthesia. Thin-cut, 2-mm-thick, postcontrast axial MR images of the brain were obtained after coordinate frame and fiducial box placement. Each target lesion was carefully contoured in the axial plane, with confirmation in the coronal and sagittal planes. Spatial coordinates in the x-, y-, and z-axes were assigned to each separate treatment target on the basis of the volumetric center of each lesion within a 3D Cartesian field. Tumor diameter and volume were also calculated for each lesion as part of the GKRS workflow. Subsequent planning of isometric shots and automated treatment of each lesion with the GKRS machine was then performed. The Leksell coordinate frame was removed after the procedure. The accuracy of this frame-based localization process, coupled with the consistent application of the stereotactic head frame from patient to patient, enabled utilization of objective coordinate data for topographic pattern analysis. For the purposes of this study, patients with treated brain metastasis arising from 1 of 5 common primary tumor origins (breast, colon, lung, skin, and kidneys) were included in the study population.

Because coordinate data were derived from a stereotactic head frame, we adjusted for variations due to each patient's head size and frame placement. For interpretability and statistical modeling, these individual dimensions were translated to a common reference frame. Translation shifted the x-, y-, and z-axes to correspond to the midsagittal, midcoronal, and midtransverse planes of the brain, respectively, by the overall mean x, y, and z values, i.e., $(\bar{x}, \bar{y}, \bar{z})$, which corresponded to the (0, 0, 0) point.

Some patients underwent multiple GKRS procedures. To account for the potential impact of treatment on localization of subsequent or future metastasis, which could bias the estimation of spatial profiles, only data from initial treatments were included. Many patients had multiple metastases measured during initial treatment, all of which were included in the

model. Additional data parameters collected for each treatment included age, sex, tumor volume, and treatment date.

Development of Topographic Prediction Models

We utilized spatial generalized additive models (GAMs) to analyze GKRS coordinate data. From these, we developed RBMEM and BRSM. GAMs are regression models that allow for predictors to be defined as smooth functions specified by nonparametric basis functions; in this case, tensor product regression splines. Semiparametric GAMs include both smooth and linear function parameterizations. In spatial statistics, GAM models are widely used to characterize spatial processes and interpolate point-referenced (geostatistical) data. We adopted spatial GAM to specify a tensor product spline on the basis of the GKRS locations centered on the x-, y-, and z-axes.

We used two approaches. The first used multinomial logistic GAM specified as

$$y_{ki} = \beta_{k0} + f(x_{ki}, y_{ki}, z_{ki}) + \beta_{k1}u_{ki} + \beta_{k2}v_{ki} + \beta_{k3}w_{ki} + \varepsilon_{ki} \quad \text{[Eq. 1]}$$

where y_{ki}, is the nominal outcome variable identifying the kth primary cancer type (breast, colon, lung, melanoma, or renal) for patient i, f is a 3D smooth function defined by the tensor product spline of a patient's centered GKRS coordinates (x_{ki}, y_{ki}, z_{ki}), β_{k0} is the intercept, β_{k1} is the linear parameter for age (u), β_{k2} is the linear parameter for sex (v), and β_{k3} is the linear parameter for tumor volume (w). The residual, ε_{ki}, is distributed as

$$Pr_i(k) = \frac{e^{\theta_{ki}}}{\sum \in C_i e^{\theta_i}} \quad \text{[Eq. 2]}$$

where θ_{ki} includes the linear and smooth terms shown in Eq. 1 and were estimated with penalized likelihood.[5] Multinomial RBMEM enabled us to test the null hypothesis that tumor localization does not vary according to cancer diagnosis, and the results of this model provided predicted probabilities of regional tumor localization for each of the 5 examined cancer types relative to each other. For example, if the probability of tumor localization to the frontal lobe was 75% for melanoma according to RBMEM, the probabilities of metastasis to that region for colon, breast, renal, and lung cancers would sum to 25%. Therefore, these probabilities are partially constrained by the relative distributions of cancers within our given data set, but nevertheless provide spatial predictions of tumor localization.

In the second approach, we separately examined the spatial patterns of metastasis for each cancer type with stratified logistic regression. BRSM assessed the likelihood of a selected cancer type to metastasize to various brain regions, independent of other cancer types. In BRSM, the observed tumor coordinates were compared with those of a spatially random reference group. A set of 500 spatially random tumors was generated with random sampling of the x, y, and z coordinates inside a sphere defined by the limits of the observed patient coordinates. This approach enabled comparison of spatial metastasis patterns with a scenario in which there was no preferential topographic pattern, thereby separately testing the null hypothesis that tumor localization was not different than a spatially random process.

Within-patient confounding in each patient by a random effect was also explored in the multinomial GAM framework to ensure that our focus on data from initial treatments was sound. From the fitted models, the predicted probabilities were visualized on a spatially gridded “mesh” that consisted of the 3 axes of 2D brain slices (sagittal, coronal, and transverse planes) that had been generated with the R package ggBrain. For interpretation, we also applied the fitted models to predict the probability of tumor presence at known coordinates representing specific regions of the brain. See Supplemental Material for the results of model sensitivity analyses.

Statistical Analysis

Summary statistics were presented as mean ± SD or number (percent). RBMEM and BRSM results were presented as OR (95% CI). The impaired student t-test (2-tailed) was used for comparisons of the two groups. For multiple-group analysis, we used 1-way ANOVA with Bonferroni adjustment.

Results

Characteristics of the Patient Population

A total of 973 patients with 3196 unique brain metastatic lesions arising from the top 5 primary systemic tumor origins (breast, colon, lung, skin, and kidneys) were screened. The observed stereotactic, volumetric Cartesian coordinates obtained from the Leksell coordinate frame in the x, y, and z planes at the time of GKRS treatment were recorded for each individual with colon, renal cell, breast, melanoma, and lung metastatic lesions (n = 2106; Fig. 1).

Patients received as many as 9 separate treatments, with 66% receiving only 1 GKRS treatment, 23% receiving 2 treatments, and 7% receiving 3 or more treatments. The mean numbers of GKRS treatments were 1.5, 1.3, 1.4, 1.7, and 1.7 for patients with breast, colon, lung, melanoma, and renal tumors, respectively. Restriction of our analysis to each patient’s initial GKRS treatment resulted in an analytical sample of 2106 unique metastases from 967 patients (Table 1). The included brain metastasis patients had the following primary cancer types: melanoma (483 patients [50%]), lung (226 [23%]), breast (134 [14%]), renal cell carcinoma (89 [9%]), and colon (33 [3%]). Renal, melanoma, and colon metastases were predominantly in male patients (83%, 67%, and 54% of patients, respectively), whereas breast and lung cancer metastases were predominantly in female patients (99% and 53% of patients, respectively). The mean ± SD number of metastases per patient was greatest for lung cancer (2.5 ± 2.9) and least for colon cancer (1.6 ± 0.85). Breast cancer patients tended to be younger (52.9 ± 10.6 years), whereas colon cancer patients tended to be older (63.9 ± 10.0 years).

Relationships Among Cancer Subtype, Neuroanatomical Regionalization, and Patient Age and Sex

The age-adjusted multinomial GAM showed that younger breast cancer patients had statistically higher odds of brain metastasis (OR [95% CI] 0.98 [0.97–0.99]); patients with all other cancer types had increased odds per unit increase in age (Supplemental Material).

We then asked whether any age differentiation was observed, given the predicted regionalization of brain metastasis by cancer subtype. Our results showed that breast cancer patients with frontal lobe metastasis were significantly younger than patients with colon (52.8 vs 68.9 years, $p = 0.0003$), lung (52.8 vs 61.1 years, $p < 0.0001$), and renal (52.8 vs 60.5 years, $p = 0.0007$) metastases in the frontal lobe (Fig. 2A). Furthermore, melanoma patients with frontal lobe metastasis were significantly younger than patients with lung (56.7 vs 61.1 years, $p = 0.0002$) and colon (56.7 vs 68.9 years, $p = 0.08$) metastases in the frontal lobe (Fig. 2A). Among patients with metastasis to the parietal lobe, breast cancer patients were significantly younger than patients with colon (50.44 vs 64.3 years, $p = 0.0204$), lung (50.44 vs 59.8 years, $p < 0.001$), melanoma (50.44 vs 55.8 years, $p = 0.0459$), and renal cell (50.44 vs 59.7 years, $p = 0.0049$; Fig. 2B) tumors. Lung cancer patients with parietal lobe metastasis were significantly older than melanoma patients (59.8 vs 55.8 years, $p = 0.0301$; Fig. 2B). Similarly, among those with metastasis to the temporal lobe, lung cancer patients were significantly older than melanoma patients (61.4 vs 55.9 years, $p = 0.0044$; Fig. 2C). Among those with occipital lobe metastasis, lung cancer patients were significantly older than patients with breast cancer (61.6 vs 52.4 years, $p = 0.001$) and melanoma (61.6 vs 56.4 years, $p = 0.0205$; Fig. 2D). Among those with cerebellar metastasis, breast cancer patients were significantly younger than patients with colon (52.8 vs 64.9 years, $p = 0.0018$), lung (52.8 vs 61.0 years, $p < 0.0001$), and melanoma (52.8 vs 58.2 years, $p < 0.0001$; Fig. 2E) tumors. Overall, there were significance differences in age and cancer subtypes for each neuroanatomical lobe. These results may open up further research discussions about age-dependent factors that may contribute to disease-specific spread in each lobe.

In addition, the sex-adjusted multinomial GAM revealed that the odds of brain metastasis in renal cancer patients was higher for males (OR [95% CI] 4.17 [2.69–6.44]), whereas the odds of brain metastasis in colon and lung cancer patients was higher for females (OR $[95\% CI]_{colon}$ 0.84 [0.74–1.52]; OR $[95\% CI]_{lung}$ 0.70 [0.53–0.87]; Supplemental Material). Overall, there was no significant difference in the numbers of brain metastatic lesions between male and female patients (Supplemental Material). However, when tumors were stratified according to primary disease site, only metastasis from renal cell carcinoma to the brain demonstrated significantly different numbers of lesions per patient between sexes (mean 2.0 for males vs 1.5 for females, $p = 0.043$; Supplemental Material).

Association Between Tumor Volume and Spatial Distribution Patterns of Brain Metastasis

Tumor volumes were significantly larger for colon cancer patients (4.8 cm^3) compared with those of patients with all other tumors, which ranged from 2.2 to 2.9 cm^3 (Table 1). Accordingly, the odds of larger volume of brain metastasis were statistically significant for patients with colon (OR [95% CI] 1.10 [1.05–1.15]) and breast (OR [95% CI] 1.04 [1.01–1.07]) cancers compared with that of patients with melanoma (Supplemental Material).

We then assessed the relationship between tumor volume and CNS topography in 9 anatomical locations (basal ganglia, brainstem, cerebellum, frontal lobe, occipital lobe, parietal lobe, temporal lobe, thalamus, and ventricular regions; Supplemental Material). The results showed that melanoma, colon, renal, and breast metastases were not significantly different in terms of tumor volumetric size across the 9 anatomical landmarks, whereas lung

cancer had significantly decreased metastatic volume in subdural mater relative to volume in the frontal, occipital, and parietal lobes. Interestingly, colon cancer patients did not have brain metastases in the basal ganglia, brainstem, or ventricular regions, and renal cancer did not metastasize to the basal ganglia or thalamic regions.

Results of RBMEM

Utilizing multinomial GAM, RBMEM enabled us to assess relative differences in probability of metastasis to preselected brain regions (frontal lobe, parietal lobe, temporal lobe, occipital lobe, cerebellum, and brainstem) for the 5 primary cancer types. Distinguishing the left and right cerebral hemispheres, along with the cranial lobes (frontal, parietal, temporal, and occipital), cerebellum, and brainstem, we predicted preferential metastasis of the most common cancer types to predefined brain regions relative to all other cancer subtypes in our data set (Fig. 3).

On the basis of the GAM results, we chose stereotactic coordinates that corresponded to the center of each neuroanatomical lobe. We then defined the predicted probability of metastasis to that brain region. Topographic results showed that metastasis from lung cancer was most likely to appear in the left frontal cortex (OR [95%] 0.26 [0.12–0.41]), right parietal lobe (OR [95% CI] 0.34 [0.23–0.45]), left parietal lobe (OR [95% CI] 0.29 [0.19–0.40]), and left temporal lobe (OR [95% CI] 0.29 [0.19–0.40]; Fig. 3A and F). Melanoma had the highest probability of metastasis to the right frontal lobe (OR [95% CI] 0.76 [0.64–0.89]) and right occipital lobe (OR [95% CI] 0.72 [0.64–0.80]; Fig. 3E and F) relative to other tumor subtypes. Breast cancer had the highest probability of metastasis to the left cerebellar hemisphere (OR [95% CI] 0.27 [0.14–0.40]) and right cerebellar hemisphere (OR [95% CI] 0.27 [0.20–0.34]; Fig. 3C and F). Finally, renal cell carcinoma had the highest probability of metastasis to the brainstem (OR [95% CI] 0.15 [0.06–0.23]; Fig. 3D and F). Our results also showed that colon cancer demonstrated a distribution pattern similar to random and did not have dominant representation in any CNS location included in our data set, although this may have been due to the small number of patients with this cancer subtype (Fig. 3B). Finally, in our data set, there was no predilection for any single cancer subtype to metastasize to the left occipital lobe.

Results of BRSM

We utilized logistic GAMs to assess whether a given primary cancer was more likely to show topographic preference for metastasis, independent of other cancer subtypes in our data set. Using 500 randomly drawn spatial coordinates as a control, we generated prediction probabilities of brain metastasis (Fig. 4). We found that, compared with random tumor locations, lung cancer had the highest propensity to metastasize to the left (OR [95% CI] 0.67 [0.47–0.82]) and right (OR [95% CI] 0.77 [0.61–0.88]; Fig. 4A) temporal lobes. Breast cancer had the highest proclivity for metastasis to the right cerebellar hemisphere (OR [95% CI] 0.83 [0.70–0.91]; Fig. 4B). Melanoma had the highest probability of metastasis to the left temporal lobe (OR [95% CI] 0.89 [0.81–0.94]; Fig. 4C). Colon cancer had the highest probability of metastasis to the right cerebellar hemisphere (OR [95% CI] 0.45 [0.26–0.65]; Fig. 4D). Finally, renal cell carcinoma had the highest predilection for spread to the brainstem (OR [95% CI] 0.47 [0.27–0.68]; Fig. 4E).

Discussion

Improved understanding of topographic patterns of brain metastasis by cancer subtype may play a major role in the prevention and treatment of this common disease. Improved understanding of the role of the brain microenvironment and potential signaling markers may have major implications for improving the incidence of CNS cancer involvement and overall outcomes in these patients. Recent studies have examined spatial distribution of brain metastasis with quantification based on primarily frequency alone.[6–8] In the current study, we leveraged objective spatial coordinates from a large data set of brain metastasis patients treated with GKRS, and we used two novel predictive models to test complimentary assessments of topographic distribution of metastasis based on preselected brain regions (RBMEM) or primary cancer subtype (BRSM). We identified distinctive and highly predictive patterns of the topographic distributions of metastasis based on both predefined cancer of origin and brain region in patients with melanoma, breast, lung, colon, and renal cell cancers.

Overall, we found that lung cancer and melanoma showed higher propensities for metastasis to the frontal and temporal lobes. On the other hand, breast, renal, and colon cancers showed higher likelihoods of spread to the hindbrain regions, notably the cerebellum and brainstem. These tumor-specific CNS topographic patterns may underlie the ability of cancer cells to adapt to regional neural microenvironments in order to facilitate colonization and thereby establish and enable progression of brain metastasis. Such a microenvironment that caters to metastatic foci formation and outgrowth is often referred to as a metastatic niche.[9] Recent studies have established that the physiological microenvironment of the brain must become a tumor-favorable niche in order for successful colonization by metastatic cancer cells.[10–17]

Neurons utilize classic neurotransmitters (e.g., glutamate, GABA, acetylcholine, dopamine, serotonin) to propagate signals for rapid communication. However, neuromodulators such as GABA and glutamate are multifunctional and may also be used by the cells of various organs outside the CNS. Thus, differential response to neurotransmitters by non-CNS tumors merits investigation. Our results show that breast cancer metastasis is statistically more likely to arise in the cerebellum For example, GABA is the predominant inhibitory neurotransmitter in the adult brain, and it is crucial for the development of cerebellar function and GABAergic synapses.[18] Although GABA is distributed throughout the brain parenchyma, GABA and GABAergic communication is predominant in the cerebellum.[18] Recent studies have shown that breast-to-brain metastasis displays enhanced expression of GABAergic variables (e.g., GABA receptors, GABA transporters, synthetic GABA enzymes). Breast-to-brain metastasis can also use GABA at physiological concentrations as an oncometabolite for proliferation.[12] In conjunction with our topographic finding regarding the predilection of breast cancer metastasis to the cerebellum, these data suggest that the cerebellum provides a conducive microenvironment for incoming breast cancer cells that can adapt to a GABA-rich neural environment.

Our data also show the topographic propensity of melanoma to metastasize to the right frontal lobe. Biologically, neurons and melanomas are both derived from the neural crest. Invasive melanomas frequently exhibit a neuron progenitor–like and early brain–adaptive

phenotype, which potentially facilitate CNS colonization.[19] Glutamine is imperative for the survival and proliferation of melanoma (glutamine addiction),[20] and malignant melanoma cells show enhanced expression of glutamate receptors. Glutamine is also abundantly found in the brain, where it is used as a substrate for the synthesis of glutamate and/or GABA and also directly participates in neurotransmission by binding to NMDA receptors.[21] Both glutamate and glutamine are found at higher concentrations in the normal brain cortex than the cerebellum, with a high concentration of glutamate in the gray matter of the right frontal lobe and a high concentration of glutamine in the white matter of the right frontal lobe.[22] We hypothesize that this glutamate/glutamine distribution may be associated with the identified topographic distribution of metastatic melanoma lesions in the brain, particularly within the right frontal lobe.

Although our data show a broad spatial distribution of lung metastasis within the brain, this tumor subtype nevertheless showed a strong statistical proclivity for spread to the bilateral temporal and parietal lobes. Lung cancer is an inherently aggressive primary tumor. Fifty percent of patients with lung cancer have brain metastasis at the time of disease presentation, and sometimes the CNS is the sole site of dissemination.[23,24] This raises the possibility that malignant lung cancer cells that penetrate the parenchyma through the blood-brain barrier may hijack the metastatic CNS niche more easily than other cancers, rather than gradually developing a neuro-adaptive phenotype.

In the current work, the subset of brain metastases amenable to GKRS was by definition a self-selected group of metastases that tend to be smaller than the lesions seen in patients who undergo surgical intervention, thereby potentially introducing an element of selection bias to this study and limiting its generalizability to all patients with brain metastasis. Nevertheless, the sheer volume of brain metastases included in this study and the use of objective spatial coordinate data offer a novel and significant degree of statistical power that has never been leveraged in order to use spatial GAM analysis to study the topographic distributions of brain metastases.

Conclusions

Nonuniform spatial distribution of metastasis to preferential brain regions varies according to primary cancer subtype in patients treated with GKRS, as validated by two novel complementary spatial models based on preselected brain region or primary cancer subtype. Melanoma and lung cancer showed predilections for metastasis to the frontal and temporal lobes, but breast, renal, and colon cancers showed preferential patterns of spread to hindbrain regions. These cancer-specific CNS topographic patterns may underlie the ability of metastatic cells to adapt to regional neural microenvironments in order to facilitate colonization and establish brain metastasis.

Supplementary Material

Refer to Web version on PubMed Central for supplementary material.

Acknowledgments

Dr. Neman, Ms. Deshpande, and Dr. Franklin are supported by a Susan G. Komen Career Catalyst Grant (CCR15332673), National Institutes of Health/National Cancer Institute (1R01CA223544-01A1), Department of Defense Breast Cancer Research Program (BC141728), and METAvivor.

ABBREVIATIONS

BRSM	brain region susceptibility model
GAM	generalized additive model
GKRS	Gamma Knife radiosurgery
RBMEM	regional brain metastasis echelon model

References

1. Deshpande K, Buchanan I, Martirosian V, Neman J. Clinical perspectives in brain metastasis. Cold Spring Harb Perspect Med. 2020;10(6):a037051. [PubMed: 31615863]
2. Peinado H, Zhang H, Matei IR, et al. Pre-metastatic niches: organ-specific homes for metastases. Nat Rev Cancer. 2017;17(5):302–317. [PubMed: 28303905]
3. Termini J, Neman J, Jandial R. Role of the neural niche in brain metastatic cancer. Cancer Res. 2014;74(15):4011–4015. [PubMed: 25035392]
4. Chang EL, Wefel JS, Hess KR, et al. Neurocognition in patients with brain metastases treated with radiosurgery or radiosurgery plus whole-brain irradiation: a randomised controlled trial. Lancet Oncol. 2009;10(11):1037–1044. [PubMed: 19801201]
5. Wood SN. On confidence intervals for generalized additive models based on penalized regression splines. Aust N Z J Stat. 2006;48(4):445–464.
6. Delattre JY, Krol G, Thaler HT, Posner JB. Distribution of brain metastases. Arch Neurol. 1988;45(7):741–744. [PubMed: 3390029]
7. Mampre D, Ehresman J, Alvarado-Estrada K, et al. Propensity for different vascular distributions and cerebral edema of intraparenchymal brain metastases from different primary cancers. J Neurooncol. 2019;143(1):115–122. [PubMed: 30835021]
8. Takano K, Kinoshita M, Takagaki M, et al. Different spatial distributions of brain metastases from lung cancer by histological subtype and mutation status of epidermal growth factor receptor. Neuro Oncol. 2016;18(5):716–724. [PubMed: 26519739]
9. Achrol AS, Rennert RC, Anders C, et al. Brain metastases. Nat Rev Dis Primers. 2019;5(1):5. [PubMed: 30655533]
10. Neman J, Choy C, Kowolik CM, et al. Co-evolution of breast-to-brain metastasis and neural progenitor cells. Clin Exp Metastasis. 2013;30(6):753–768. [PubMed: 23456474]
11. Neman J, Somlo G, Jandial R. Classification of genomic changes in breast cancer brain metastasis. Neurosurgery. 2010;67(2):N18–N19. [PubMed: 20644404]
12. Neman J, Termini J, Wilczynski S, et al. Human breast cancer metastases to the brain display GABAergic properties in the neural niche. Proc Natl Acad Sci U S A. 2014;111(3):984–989. [PubMed: 24395782]
13. Choy C, Ansari KI, Neman J, et al. Cooperation of neurotrophin receptor TrkB and Her2 in breast cancer cells facilitates brain metastases. Breast Cancer Res. 2017;19(1):51. [PubMed: 28446206]
14. Priego N, Zhu L, Monteiro C, et al. STAT3 labels a subpopulation of reactive astrocytes required for brain metastasis. Nat Med. 2018;24(7):1024–1035. [PubMed: 29892069]
15. Zhang L, Zhang S, Yao J, et al. Microenvironment-induced PTEN loss by exosomal microRNA primes brain metastasis outgrowth. Nature. 2015;527(7576):100–104. [PubMed: 26479035]
16. Gril B, Paranjape AN, Woditschka S, et al. Reactive astrocytic S1P3 signaling modulates the blood-tumor barrier in brain metastases. Nat Commun. 2018;9(1):2705. [PubMed: 30006619]

17. Contreras-Zárate MJ, Day NL, Ormond DR, et al. Estradiol induces BDNF/TrkB signaling in triple-negative breast cancer to promote brain metastases. Oncogene. 2019;38(24):4685–4699. [PubMed: 30796353]
18. Takayama C Formation of GABAergic synapses in the cerebellum. Cerebellum. 2005;4(3):171–177. [PubMed: 16147949]
19. Nygaard V, Prasmickaite L, Vasiliauskaite K, et al. Melanoma brain colonization involves the emergence of a brain-adaptive phenotype. Oncoscience. 2014;1(1):82–94. [PubMed: 25593989]
20. Liao J, Liu PP, Hou G, et al. Regulation of stem-like cancer cells by glutamine through β-catenin pathway mediated by redox signaling. Mol Cancer. 2017;16(1):51. [PubMed: 28245869]
21. Liebschutz J, Airoldi L, Brownstein MJ, et al. Regional distribution of endogenous and parenteral glutamate, aspartate and glutamine in rat brain. Biochem Pharmacol. 1977;26(5):443–446. [PubMed: 849337]
22. Goryawala MZ, Sheriff S, Maudsley AA. Regional distributions of brain glutamate and glutamine in normal subjects. NMR Biomed. 2016;29(8):1108–1116. [PubMed: 27351339]
23. Popper HH. Progression and metastasis of lung cancer. Cancer Metastasis Rev. 2016;35(1):75–91. [PubMed: 27018053]
24. Greenspoon JN, Ellis PM, Pond G, et al. Comparative survival in patients with brain metastases from non-small-cell lung cancer treated before and after implementation of radiosurgery. Curr Oncol. 2017;24(2):e146–e151. [PubMed: 28490938]

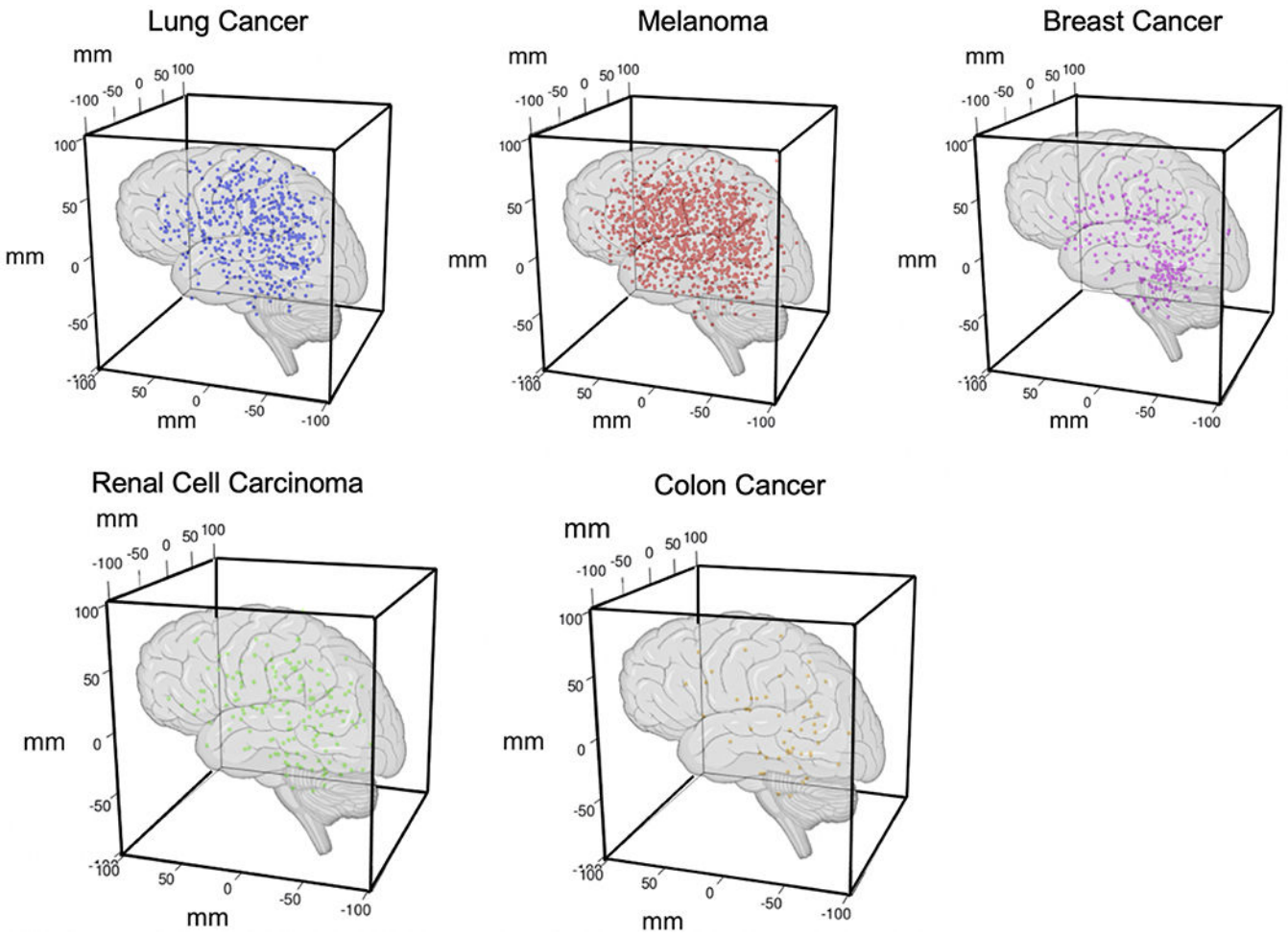

FIG. 1.

3D representations of the observed distributions of brain metastases according to primary origin. Stereotactic volumetric Cartesian coordinates obtained from the Leksell surgical coordinate frame in the x, y, and z planes at the time of GKRS treatment were recorded for each individual metastatic lesion (breast [285 lesions], colon [52], lung [502], melanoma [1099], and renal cell carcinoma [168]). Figure is available in color online only.

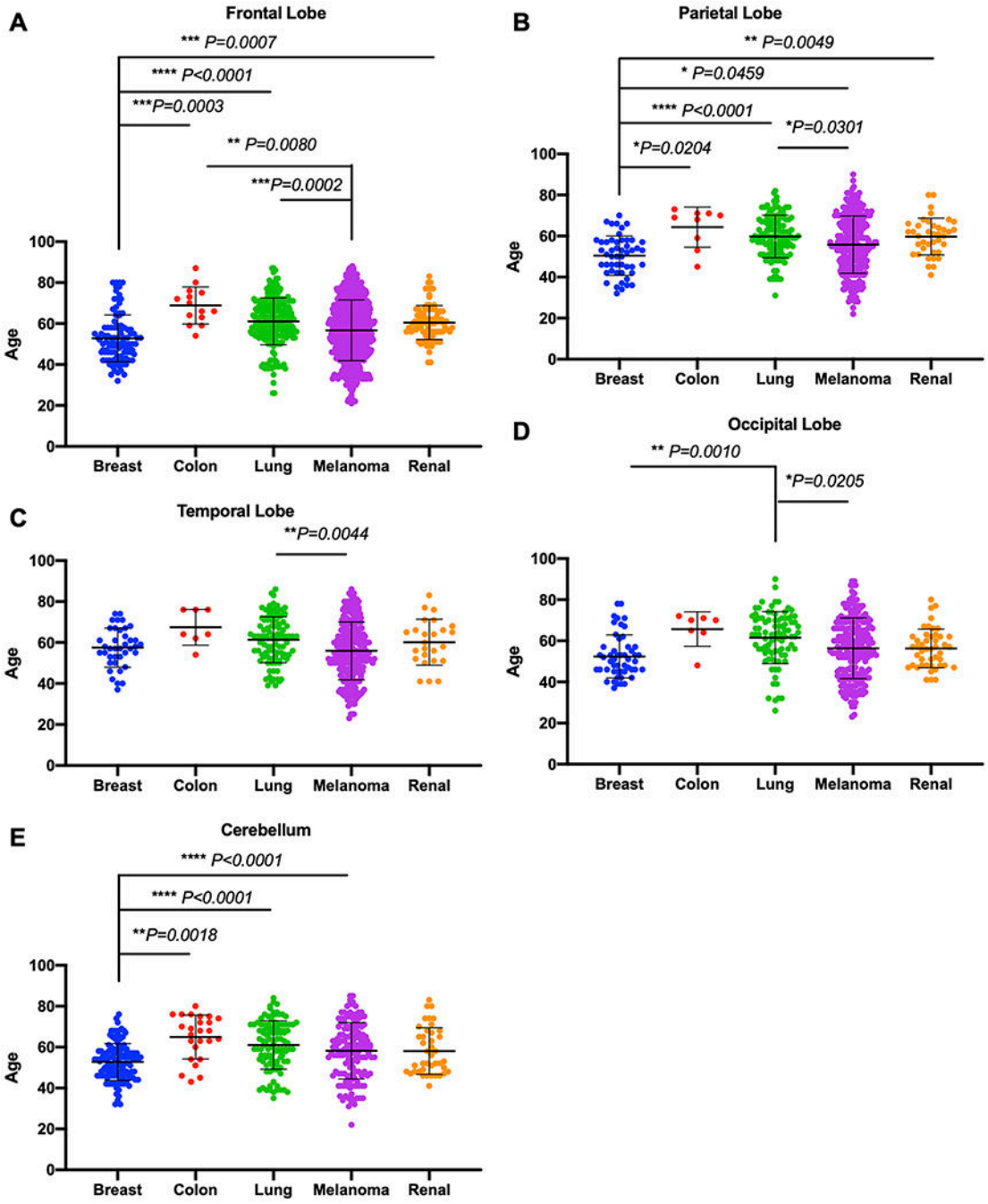

FIG. 2.

Correlations between age and brain metastasis subtype for individual neuroanatomical lobes. Given the predicted regionalization of metastasis by cancer subtype, we further examined whether age differentiation was observed. **A:** Breast cancer patients with frontal lobe metastasis were significantly younger than patients with colon ($p = 0.0003$), lung ($p < 0.0001$), and renal ($p = 0.0007$) metastasis in the frontal lobe. Furthermore, melanoma patients with frontal lobe metastasis were significantly younger than patients with lung ($p = 0.0002$) and colon ($p = 0.0080$) metastasis in the frontal lobe. **B:** Among those with

parietal lobe metastasis, breast cancer patients were significantly younger than patients with colon ($p = 0.0204$), lung ($p < 0.0001$), melanoma ($p = 0.0459$), and renal cell ($p = 0.0049$) tumors, and lung cancer patients were significantly older than patients with melanoma ($p = 0.0301$). **C:** Similarly, among those with temporal lobe metastasis, lung cancer patients were significantly older than melanoma patients ($p = 0.0044$). **D:** Among those with occipital lobe metastasis, lung cancer patients were significantly older than patients with breast cancer ($p = 0.0010$) and melanoma ($p = 0.0205$). **E:** Among those with cerebellar metastasis, breast cancer patients were significantly younger than patients with colon ($p = 0.0018$), lung ($p < 0.0001$), and melanoma ($p < 0.0001$) tumors. Figure is available in color online only.

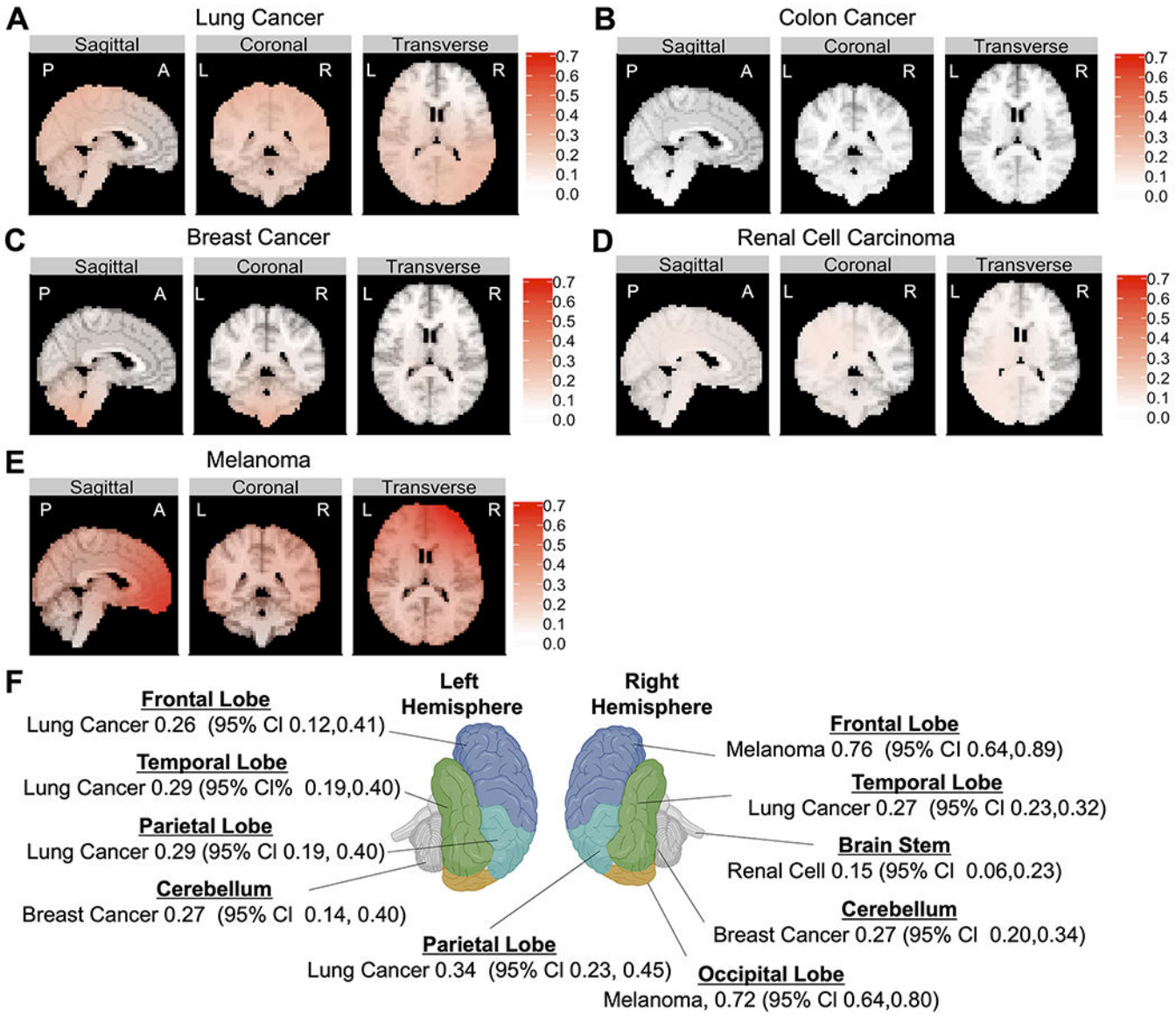

FIG. 3.

The results of RBMEM indicated the hierarchical distribution of metastasis to preselected brain regions relative to other primary cancers. Multinomial analysis was used to determine which of the preselected brain regions (frontal, parietal, temporal, and occipital lobes; cerebellum; and brainstem) were most likely to be metastasized from 5 primary cancers. **A:** Topographic results show that lung-to-brain metastasis was most likely to occur in the left frontal cortex, right parietal lobe, left parietal lobe, and left temporal lobe. **B:** Colon cancer demonstrated a distribution pattern similar to random and did not have dominant representation in any CNS location. **C:** Breast cancer had the highest probability of metastasis to the right and left cerebellar hemispheres. **D:** Renal cell carcinoma had the highest probability of metastasis to the brainstem. **E:** Melanoma had the highest probability of metastasis to the right frontal lobe and right occipital lobe relative to other tumor subtypes. **F:** Topographic illustration of the CNS showing the primary cancers with the

highest probabilities of metastasis to stereotactic coordinates corresponding to the center of each neuroanatomical lobe. Figure is available in color online only.

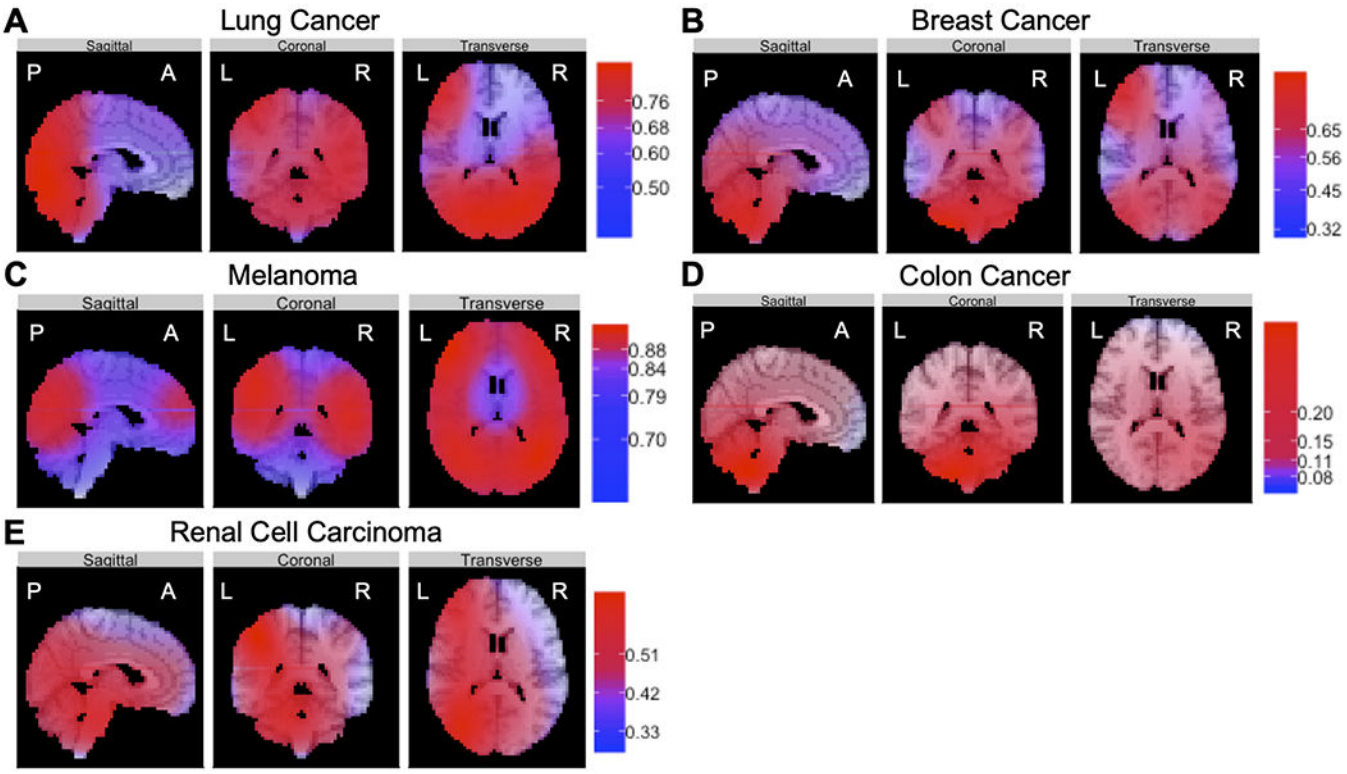

FIG. 4.

The results of BRSM revealed that primary cancers, independent of each other, had defined topographic distributions of metastasis to specific brain regions. Using fitted models to generate prediction probabilities for these brain regions, we found that lung cancer (**A**) had the highest propensity to metastasize to the left and right temporal lobes, breast cancer (**B**) had the highest proclivity for metastasis to the right cerebellar hemisphere, melanoma (**C**) had the highest probability of metastasis to the left temporal lobe, colon cancer (**D**) had the highest probability of metastasis to the right cerebellar hemisphere, and renal cell carcinoma (**E**) had the highest predilection for spread to the brainstem. Figure is available in color online only.

TABLE 1.

Characteristics of the study population

Characteristic	Cancer Subtype				
	Breast	**Colon**	**Lung**	**Melanoma**	**Renal**
No. of patients	134 (14)	33 (3)	226 (23)	483 (50)	89 (9)
Metastatic lesions					
Total	285 (14)	52 (2)	502 (24)	1099 (52)	168 (8)
No./patient	2.1 ± 1.4	1.6 ± 0.85	2.5 ± 2.9	2.3 ± 1.7	1.9 ± 1.4
Tumor vol, cm^3	2.9 ± 4.2	4.8 ± 5.0	2.6 ± 4.5	2.2 ± 4.2	2.5 ± 3.6
Age, yrs	52.9 ± 10.6	63.9 ± 10.0	60.3 ± 11.7	56.5 ± 14.6	60.8 ± 9.50
Sex					
Male	2 (1)	28 (54)	238 (47)	733 (67)	140 (83)
Female	283 (99)	24 (46)	264 (53)	366 (33)	28 (17)

Values are shown as number (percent) or mean ± SD.